Y. Bai, J.D. Biggs, Z. Zhang, Y. Ding
Adaptive Fault-Tolerant Control for Longitudinal Motion of Supercavitating Vehicles
European Journal of Control, In press - Published online 12/07/2020
doi:10.1016/j.ejcon.2020.06.002

Adaptive Fault-Tolerant Control for Longitudinal Motion of Supercavitating Vehicles

Yuliang Bai[a,*], James D. Biggs[b], Zichen Zhang[a], Yibo Ding[a]

[a]*School of Astronautics, Harbin Institute of Technology, Mailbox 345, Harbin, 150001, China.*
[b]*Department of Aerospace Science and Technology, Politecnico di Milano, Milano, 20156, Italy.*

Abstract

A supercavitating underwater vehicle uses gas or vapor to reduce its skin friction enabling it to travel up to speeds of 200 m/s. However, traveling at extreme speeds can be challenging for control design since sudden disturbances or faults, even for a short time, can lead to large deviations from the reference trajectory. This paper addresses the problem of controlling a supercavitating vehicle which incorporates the actuator constraints and loss of effectiveness of the cavitator. An adaptive control law is designed based on the backstepping control method which includes an adaptive fault-tolerant component. The bounded adaptive update law can estimate the upper bound of the unknown total uncertainties including those induced by actuator faults. The proposed control is shown to guarantee stability in the presence of faults by using Lyapunov theory.

Keywords: Supercavitating vehicles, Adaptive Control, Backstepping Control, Bounded Adaptive Update Law; Adaptive Fault-tolerant

1. Introduction

Cavitation vehicles refer to underwater vehicles that use gas or vapor in order to reduce skin friction drag[1]. Supercavitating vehicles are cavitation vehicles that operate at extremely high-speed speeds relative to a fully-wetted underwater vehicle. Although the concept of supercavitation

*Corresponding author

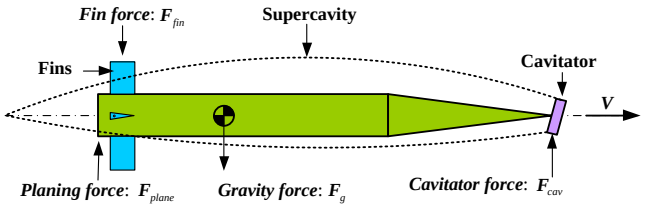

Figure 1: Forces acting on a supercavitating vehicle

has considerable potential, there are significant technical challenges related to their control[2]. Moreover, a fully-wetted underwater vehicle can use the lift generated by the body to balance the gravity, that is, it can be designed to be neutrally buoyant. However, a supercavitating vehicle cannot exploit buoyancy and, therefore, upthrust can only be delivered using the cavitator, fins and a force generated by the tail passing through the cavitation bubble wall (see Fig.1). For different velocity ranges, Y.N. Savchenko[1] proposed four stable motion modes for a supercavitating vehicle. The stable motion modes considered in the range 50-200 m/s are of particular interest for the nominal operating phase. In this paper, the mathematical model and analysis of this mode are considered.

The actuation of supercavitating vehicles can be undertaken using both a cavitator and a tail rudder. The dynamics of the supercavitating vehicle and the control inputs are highly nonlinear and can experience considerable uncertainties such as cavitation number and planing force of the tail[6]. Various control designs have been developed for supercavitating vehicles based on benchmark control[3], sliding mode control[4, 5, 6], backstepping control[7, 8], adaptive control[9, 10], linear quadratic regulator (LQR) control[11], feedback linearization[12, 13, 14], linear parameter varying (LPV) control[15, 16] and robust control[17, 18, 19]. Additional complexities in the model have been considered in the control design such as uncertainty in the slope of the fin force with respect to the fin angle of attack and the delay effect due to cavity vehicle interaction[10, 20], as well as measurement noise and cavity shape uncertainty[15].

In all previous work on supercavitating vehicles the fin and cavitator are assumed to function perfectly throughout their entire operation. However, the cavitator is subjected to a tremendous amount of hydrodynamic force and fluid pressure which could lead to uncertainty in modeling and loss of effectiveness. In addition, due to the wrapping effect of cavitation, the fin

may not be completely immersed in water, reducing the control efficiency leading to a partial loss of effectiveness[10].Since, supercavitating vehicles travel at high velocities (50-200m/s), loss of stability could be catastrophic since a large deviation from the reference trajectory may not recoverable. Thus, a fault-tolerant-control (FTC) should be developed to avoid loss of effectiveness of the fins and inefficiencies caused by the bubble wrap actuators. Various types of fault-tolerant-controls (FTC) have been developed for rigid-body vehicles including the orbit and attitude control of spacecraft[22, 23, 24, 25, 26, 27, 28, 29, 30], reentry vehicles[31, 32, 33, 34], flexible aircraft[35], quadrotors[36] and hypersonic gliding vehicles[37]. However, there have been no FTC developed for supercavitating vehicles that ensures tracking performance in the presence of faults.

In this paper, a position and attitude control is designed that guarantees stability of the supercavitating vehicle in the presence of faults and uncertainties. This is achieved by developing a control based on the backstepping method[7, 8], which is augmented with an adaptive fault-tolerant component. This paper presents a novel design of a bounded adaptive update law to estimate the upper bound of unknown total uncertainties, including parameter uncertainties, actuator faults and saturation limits. A theoretical proof of the stability of the closed-loop system of the supercavitating vehicle in the presence of faults and modeling uncertainties is given.

2. Modeling of a Supercavitating vehicle

The supercavitating vehicle concept and the corresponding reference frames used in this paper are shown in Fig.2. There are two coordinate systems used, (i) an inertial reference frame $O_eX_eY_eZ_e$ which has the origin at sea level zero, (ii) the body-fixed frame $O_bx_by_bz_b$. The origin of the body-fixed frame is located at the center of pressure of the cavitator, the x_b-axis points along the vehicle axis of symmetry, the y_b-axis points starboard and the z_b-axis points downwards. The cavitator is installed at the nose of the vehicle which can generate various cavitations at different speeds. For a cavitation of this design, the tail of vehicle will generate the lift force at the contact point (the body's tail interacts with the internal cavity surface). Since the lift force of the tail and cavitator can both compensate for buoyancy loss, the stability of the vehicle is possible.

In the presented model, the effect of time delay cavity shape has been neglected. For supercavitating vehicles, a time delay exists and can be incor-

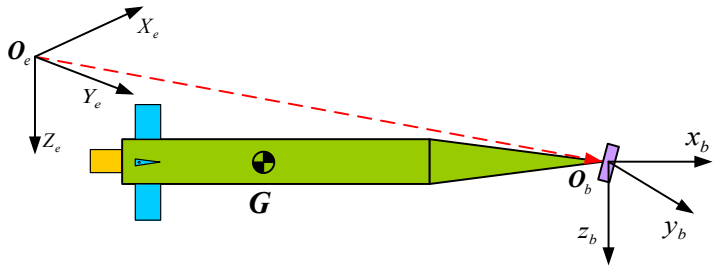

Figure 2: Configuration of the supercavitating vehicle and reference frame

porated into the planing force model. However, the planing force cannot be measured directly and must estimated. The estimation of the planing force is beyond the scope of this paper and will be considered in the future research. In this paper, a nominal planing force model is used for feedforward compensation in the control algorithm which can be replaced with a more accurate estimation using adaptive techniques.

Assuming the velocity V along the x_b-axis is constant, the dive-plane kinematics and dynamics of the rigid vehicle considering the fluid force are given by

$$\begin{aligned} \dot{z} &= w\cos\theta - V\sin\theta \\ \dot{\theta} &= q \end{aligned} \tag{1}$$

where z is the position of Z_e direction in inertial coordinates, w is the velocity of y_b-axis, θ is the pitch angle and q is the pitch angular velocity.

$$\begin{bmatrix} M & -Mx_{cg} \\ -Mx_{cg} & I_y \end{bmatrix} \begin{bmatrix} \dot{w} \\ \dot{q} \end{bmatrix} = qV \begin{bmatrix} M \\ -Mx_{cg} \end{bmatrix} + \begin{bmatrix} F_z \\ M_z \end{bmatrix} \tag{2}$$

where M is the mass of vehicle, x_{cg} is the gravity center position of x_b-axis, I_y is the inertia of y_b-axis, F_z and M_z are total forces and moments of z_b-axis, where

$$\begin{aligned} M &= \frac{7}{9} m\rho\pi R^2 L \\ x_{cg} &= -\frac{17}{28} L \\ I_y &= I_y\,(cone) + I_y\,(cylinder) \\ &= \frac{11}{60} m\rho\pi R^4 L + \frac{133}{405} m\rho\pi R^2 L^3 \end{aligned}$$

where, m is density ratio (ρ_b/ρ), ρ_b is the density of the vehicle and ρ is the the density of the fluid (sea water), L is the length of vehicle and R is the

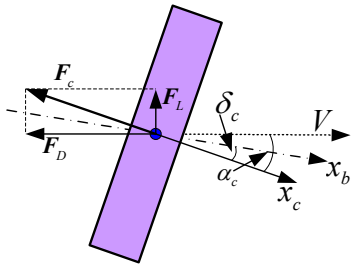

Figure 3: Cavitator angle of attack and deflection angle

radius of cylindrical body part. The above parameters are from literature [9].

$$F_z = F_{z,g} + F_{z,fin} + F_{z,cav} + F_{z,plane} \tag{3}$$

$$M_z = M_{z,g} + M_{z,fin} + M_{z,plane} \tag{4}$$

where $F_{z,g}, F_{z,fin}, F_{z,cav}, F_{z,plane}$ are components of the gravity force, fin force, cavitator force and planing force; $M_{z,g}, M_{z,fin}, M_{z,plane}$ are components of the gravity, fin and planing moment acting along the z_b-axis, where

$$\begin{aligned} F_{z,g} &= Mg\cos\theta \\ M_{z,g} &= -x_{cg}Mg\cos\theta \end{aligned} \tag{5}$$

In this paper, a disk cavitator is modelled as shown in Fig.3. The lift and drag forces of the cavitator are then given by

$$\begin{aligned} F_L &= \tfrac{1}{2}\rho V^2\pi R_n^2 C_{x0}\left(1+\sigma\right)\cos\alpha_c\sin\alpha_c \\ F_D &= \tfrac{1}{2}\rho V^2\pi R_n^2 C_{x0}\left(1+\sigma\right)\cos^2\alpha_c \end{aligned} \tag{6}$$

where R_n is the radius of the cavitator, C_{x0} is the drag coefficient at the zero angle of attack, σ is the cavitation number and α_c is the angle of attack defined by

$$\alpha_c = \tan^{-1}\left(\frac{w}{V}\right) + \delta_c \tag{7}$$

where δ_c is the deflection angle of the cavitator, defined to be positive in the counter-clockwise direction. Then the body-axis z-component of the cavitator force is given by

$$\begin{aligned} F_{z,cav} &= F_L\cos\left(\alpha_c-\delta_c\right) - F_D\sin\left(\alpha_c-\delta_c\right) \\ &= \frac{1}{2}\rho V^2\pi R_n^2 C_{x0}\left(1+\sigma\right)\cos\alpha_c\sin\delta_c \end{aligned} \tag{8}$$

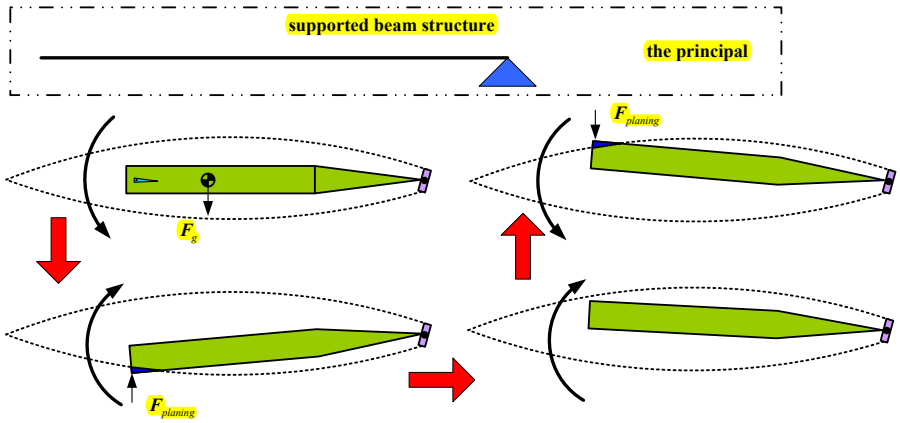

Figure 4: The generation process of tail beat phenomenon

The tail beat phenomenon produces a planing force. Moreover, if the reference point is selected to be in the center of the head cavitator, the whole system is similar to a simple supported beam structure. Under the action of the gravity moment, the tail of the vehicle will deflect downwards (as shown in Fig.4), and tail will move outside of the cavity. Due to the upward force exerted by the fluid, when the moment is greater than the gravity moment, the tail will then move towards the interior of the cavity. When the tail moves into the cavity, the planing force disappears. When the tail continually moves to the outside of the cavity, the planing force is generated again. If this is not controlled, the process will repeat, result in what is known as the oscillation phenomenon.

The model of planing force and moment adopted in this paper comes from literature[39,40], which is based on Hassan theory. Logvinovich has given the model for the cylindrical body planing force and moment. At present, there are other similar models[3,10,20]. The planing force and moment of the supercavitating vehicle is given by [39, 40]

$$\begin{aligned} F_{z,plane} &= \frac{1}{2}\pi\rho R^2 V^2 \sin\alpha_{plane}\cos\alpha_{plane}\left(\frac{R+h}{R+2h}\right)\left[1-\left(\frac{R_c-R}{h+R_c-R}\right)^2\right] \\ M_{z,plane} &= \frac{1}{2}\pi\rho R^2 V^2 \cos^2\alpha_{plane}\frac{h^2}{h+R_c-R}\frac{R+h}{R+2h} \end{aligned} \tag{9}$$

where the cavity radius R_c and its contraction rate $\dot{R}_c$, as well as the param-

eters $h^{'}$, $R^{'}$, and α_{plane} are defined by

$$\alpha_{plane} = \begin{cases} \theta - \frac{w+\dot{R}_c}{V}, & \theta > \frac{R_c - R}{L} \\ 0, & \frac{R-R_c}{L} \leq \theta \leq \frac{R_c-R}{L} \\ \theta - \frac{w-\dot{R}_c}{V}, & \theta < \frac{R-R_c}{L} \end{cases} \tag{10}$$

$$\begin{aligned} R_c &= R_n\left(0.82\tfrac{1+\sigma}{\sigma}\right)^{0.5} K_2 \\ \dot{R}_c &= \frac{-\frac{20}{17}\left(0.82\frac{1+\sigma}{\sigma}\right)^{0.5} V\left(1-\frac{4.5\sigma}{1+\sigma}\right) K_1^{23/17}}{K_2(1.92/\sigma - 3)} \end{aligned} \tag{11}$$

$$\begin{aligned} K_1 &= \tfrac{L}{R_n}\left(\tfrac{1.92}{\sigma} - 3\right)^{-1} - 1 \\ K_2 &= \left[1 - \left(1 - \tfrac{4.5\sigma}{1+\sigma}\right) K_1^{40/17}\right]^{0.5} \end{aligned} \tag{12}$$

$$h = \begin{cases} R - R_c + L\theta, & \theta > \frac{R_c - R}{L} \\ 0, & \frac{R-R_c}{L} \leq \theta \leq \frac{R_c-R}{L} \\ R - R_c - L\theta, & \theta < \frac{R-R_c}{L} \end{cases} \tag{13}$$

Denoting n to be the effectiveness of the fins relative to the cavitator, where effectiveness of the fins represents the change of the z-component force in the body axis due to a unit change of the fin angle of attack, then the z-component fin force and the fin-induced pitching moment are

$$\begin{aligned} F_{z,fin} &= -\tfrac{1}{2}\rho V^2 \pi R_n^2 C_{x0}\,(1+\sigma) n \alpha_f \\ M_{fin} &= F_{z,fin} L \end{aligned} \tag{14}$$

where α_f denotes the fin angle of attack:

$$\alpha_f = \tan^{-1}\left(\frac{w + qL}{V}\right) + \delta_f \tag{15}$$

where δ_f is the fin deflection angle.

For simplicity of exposition, let the state of the supercavitating vehicle be defined by $\boldsymbol{x}_1 = [z, \theta]^T$, $\boldsymbol{x}_2 = [w, q]^T$ and the control input $\boldsymbol{u} = [\delta_f, \delta_c]^T$, based on the above mathematical model, assuming $cos\theta \approx 1$ and $sin\theta \approx \theta$, the nonlinear model of the system is given by

$$\begin{aligned} \dot{\boldsymbol{x}}_1 &= A\boldsymbol{x}_1 + \boldsymbol{x}_2 \\ J\dot{\boldsymbol{x}}_2 &= B\boldsymbol{x}_2 + C\boldsymbol{u} + \boldsymbol{F}_g + \boldsymbol{F}_{plane} \end{aligned} \tag{16}$$

where $\boldsymbol{F}_g = [F_g, M_g]^T$, $\boldsymbol{F}_{plane} = [F_{plane}, M_{plane}]^T$ and

$$
\begin{aligned}
J &= \begin{bmatrix} M & -Mx_{cg} \\ -Mx_{cg} & I_y \end{bmatrix}, A = \begin{bmatrix} 0 & -V \\ 0 & 0 \end{bmatrix} \\
B &= \tfrac{1}{2}\rho V \pi R_n^2 C_{x0}(1+\sigma) \begin{bmatrix} -n & -nL \\ -nL & -nL^2 \end{bmatrix} + V \begin{bmatrix} 0 & M \\ 0 & -Mx_{cg} \end{bmatrix} \\
C &= \tfrac{1}{2}\rho V^2 \pi R_n^2 C_{x0}(1+\sigma) \begin{bmatrix} -n & 1 \\ -nL & 0 \end{bmatrix}
\end{aligned}
$$

3. Adaptive Backstepping Tracking Control Law Design

Initially the uncertainties in the modeling parameters and actuator faults are assumed to be bounded and an adaptive law to estimate this bound is developed. This adaptive law is then combined with a backstepping controller to track the desired motion and a proof of the closed-loop stability is provided by using a Lyapunov function.

3.1. Modeling with Uncertainties and Actuator Failures

The nonlinear model of a supercavitating vehicle described in Eq.(16) will be expressed as a known part, an uncertain part and a control input, including actuator failures and their nonlinear saturated limits:

$$
\begin{aligned}
\dot{\boldsymbol{x}}_1 &= A\boldsymbol{x}_1 + \boldsymbol{x}_2 \\
\dot{\boldsymbol{x}}_2 &= \left(\bar{B} + \Delta\bar{B}\right)\boldsymbol{x}_2 + \left(\bar{C} + \Delta\bar{C}\right)\boldsymbol{\tau} + \bar{\boldsymbol{F}}_g + \left(\bar{\boldsymbol{F}}_p + \Delta\bar{\boldsymbol{F}}_p\right)
\end{aligned}
\tag{17}
$$

where $\bar{B} = J^{-1}B, \bar{C} = J^{-1}C, \bar{\boldsymbol{F}}_g = J^{-1}\boldsymbol{F}_g$ and $\bar{\boldsymbol{F}}_p = J^{-1}F_{plane}$. The parameters $\Delta\bar{B}, \Delta\bar{C}$ and $\Delta\bar{\boldsymbol{F}}_p$ are related to the uncertainties in the modeling parameters. The control parameter $\boldsymbol{\tau}$ is subject to the following faults and saturation.

Assumption 1. *Considering two types of actuator failures of practical supercavitating vehicle,* $\boldsymbol{\Gamma}_g = \mathrm{diag}(\mathrm{g}_1, \mathrm{g}_2)$ *defines a multiplication fault which denotes efficiency of an actuator with* $0 < g_i \leq 1 (i = 1, 2)$, $\boldsymbol{\Gamma}_d = [\Gamma_{d1}, \Gamma_{d2}]^T$ *is an additive fault and satisfies* $\|\boldsymbol{\Gamma}_d\| \leq l_d$. *Since the output of the controller is bounded in practice, the actuator nonlinear saturation limit is denoted* $\boldsymbol{u}_{max}$ *and the commanded control that exceeds the saturation limit is denoted as* $\bar{\boldsymbol{u}}$. *Therefore, the real control input can be represented by*

$$
\boldsymbol{\tau} = \boldsymbol{\Gamma}_g(\boldsymbol{u} + \bar{\boldsymbol{u}}) + \boldsymbol{\Gamma}_d \tag{18}
$$

where $\bar{\boldsymbol{u}} = [\bar{u}_1, \bar{u}_2]^T$ *is bounded* $\|\bar{\boldsymbol{u}}\| \leq l_\theta$ *and satisfies*

$$\bar{u}_i = \begin{cases} \operatorname{sgn}(u_i)\, u_{max} - u_i, & |u_i| \geq u_{max} \\ 0, & otherwise \end{cases}$$

3.2. Adaptive Control Law Design

In order to track the desired signal, an adaptive backstepping tracking controller is designed. Firstly, let z_d, θ_d and w_d, q_d denote the reference signals for states z, θ, w and q, respectively. Then defining the desired state $\boldsymbol{x}_{1d} = [z_d, \theta_d]^T$ and $\boldsymbol{x}_{2d} = [w_d, q_d]^T$. Finally, the tracking error states $\tilde{\boldsymbol{x}}_1$ and $\tilde{\boldsymbol{x}}_2$ are:

$$\begin{aligned} \tilde{\boldsymbol{x}}_1 &= \boldsymbol{x}_1 - \boldsymbol{x}_{1d} \\ \tilde{\boldsymbol{x}}_2 &= \boldsymbol{x}_2 - \boldsymbol{x}_{2d} \end{aligned} \tag{19}$$

By differentiating Eq.(19) and substituting Eq.(18) into it, the tracking error differential functions can be written as

$$\begin{aligned} \dot{\tilde{\boldsymbol{x}}}_1 &= A\boldsymbol{x}_1 - \dot{\boldsymbol{x}}_{1d} + \boldsymbol{x}_2 \\ \dot{\tilde{\boldsymbol{x}}}_2 &= \left(\bar{B} + \Delta\bar{B}\right)\boldsymbol{x}_2 + \left(\bar{C} + \Delta\bar{C}\right)\boldsymbol{\Gamma}_g\boldsymbol{u} + \bar{\boldsymbol{F}}_g + \left(\bar{\boldsymbol{F}}_p + \Delta\bar{\boldsymbol{F}}_p\right) - \dot{\boldsymbol{x}}_{2d} + \left(\bar{C} + \Delta\bar{C}\right)\left(\boldsymbol{\Gamma}_g\bar{\boldsymbol{u}} + \boldsymbol{\Gamma}_d\right) \end{aligned} \tag{20}$$

In order to design a backstepping controller, we define a virtual control variable $\boldsymbol{\xi}$ as the desired value of $\tilde{\boldsymbol{x}}_2$. Defining the virtual tracking errors $\boldsymbol{e}_1 = [e_{11}, e_{12}]^T$ and $\boldsymbol{e}_2 = [e_{21}, e_{22}]^T$ as

$$\begin{aligned} \boldsymbol{e}_1 &= \tilde{\boldsymbol{x}}_1 \\ \boldsymbol{e}_2 &= \tilde{\boldsymbol{x}}_2 - \boldsymbol{\xi} \end{aligned} \tag{21}$$

Differentiating Eq.(21) and substituting in the corresponding parameters, the virtual tracking error differential functions can be expressed as

$$\begin{aligned} \dot{\boldsymbol{e}}_1 &= A\boldsymbol{x}_1 - \dot{\boldsymbol{x}}_{1d} + \boldsymbol{x}_{2d} + \boldsymbol{e}_2 + \boldsymbol{\xi} \\ \dot{\boldsymbol{e}}_2 &= \bar{B}\boldsymbol{x}_2 + \bar{C}\boldsymbol{u} + \bar{\boldsymbol{F}}_g + \bar{\boldsymbol{F}}_p - \dot{\boldsymbol{x}}_{2d} - \dot{\boldsymbol{\xi}} + \boldsymbol{E}_d \end{aligned} \tag{22}$$

where $\boldsymbol{E}_d = \Delta\bar{B}\boldsymbol{x}_2 + \left(\bar{C} + \Delta\bar{C}\right)\boldsymbol{\Gamma}_g\boldsymbol{u} - \bar{C}\boldsymbol{u} + \Delta\bar{\boldsymbol{F}}_p + \left(\bar{C} + \Delta\bar{C}\right)\left(\boldsymbol{\Gamma}_g\bar{\boldsymbol{u}} + \boldsymbol{\Gamma}_d\right)$ are the modeling parameters uncertainties, actuator failures and saturated limits.

Step 1: Designing a virtual control law as follow

$$\boldsymbol{\xi} = -\kappa_1\boldsymbol{e}_1 + \dot{\boldsymbol{x}}_{1d} - A\boldsymbol{x}_1 - \boldsymbol{x}_{2d} \tag{23}$$

where the control gain κ_1 is a positive scalar.

If there is no uncertainties and faults in Eq.(22), we can rewrite it as follows:

$$\begin{aligned}\dot{\boldsymbol{e}}_1 &= A\boldsymbol{x}_1 - \dot{\boldsymbol{x}}_{1d} + \boldsymbol{x}_{2d} + \boldsymbol{e}_2 + \boldsymbol{\xi} \\ \dot{\boldsymbol{e}}_2 &= \bar{B}\boldsymbol{x}_2 + \bar{C}\boldsymbol{u} + \bar{\boldsymbol{F}}_g + \bar{\boldsymbol{F}}_p - \dot{\boldsymbol{x}}_{2d} - \dot{\boldsymbol{\xi}}\end{aligned} \tag{24}$$

Step 2: Designing the control law as

$$\boldsymbol{u} = -\bar{C}^{-1}\left(\boldsymbol{e}_1 + \kappa_2\boldsymbol{e}_2 + \bar{B}\boldsymbol{x}_2 + \bar{\boldsymbol{F}}_g + \bar{\boldsymbol{F}}_p - \dot{\boldsymbol{x}}_{2d} - \dot{\boldsymbol{\xi}}\right) \tag{25}$$

where the control gain κ_2 is a positive scalar.

Theorem 1. *The virtual control law (23) and the feedback control law (25) guarantee that the virtual tracking errors (21) and tracking errors (19) converge to the origin as $t \to \infty$, such that $\lim_{t\to\infty} \boldsymbol{e}_1 = 0$ and $\lim_{t\to\infty} \boldsymbol{e}_2 = 0$.*

Considering Eq.(21), the backstepping tracking control law can stabilize the desired motion such that $\lim_{t\to\infty} \tilde{\boldsymbol{x}}_1 = \boldsymbol{0}$, $\lim_{t\to\infty} \tilde{\boldsymbol{x}}_2 = \boldsymbol{0}$ for any initial tracking error $[\tilde{\boldsymbol{x}}_1(0), \tilde{\boldsymbol{x}}_2(0)] \in \mathbb{R}^{2\times 2}$.

Proof: Defining the Lyapunov function as:

$$V_1 = \frac{1}{2}\boldsymbol{e}_1^T\boldsymbol{e}_1 + \frac{1}{2}\boldsymbol{e}_2^T\boldsymbol{e}_2 \tag{26}$$

The time derivative of the Lyapunov function is

$$\dot{V}_1 = \boldsymbol{e}_1{}^T\dot{\boldsymbol{e}}_1 + \boldsymbol{e}_2{}^T\dot{\boldsymbol{e}}_2 \tag{27}$$

Recalling Eq.(24) and Eq.(23), the time derivative of this Lyapunov function becomes

$$\dot{V}_1 = \boldsymbol{e}_1{}^T(-\boldsymbol{\kappa}_1\boldsymbol{e}_1 + \boldsymbol{e}_2) + \boldsymbol{e}_2{}^T(\bar{B}\boldsymbol{x}_2 + \bar{C}\boldsymbol{u} + \bar{\boldsymbol{F}}_g + \bar{\boldsymbol{F}}_p - \dot{\boldsymbol{x}}_{2d} - \dot{\boldsymbol{\xi}}) \tag{28}$$

Substituting the control law Eq.(25) into Eq.(28) gives

$$\begin{aligned}\dot{V}_1 &= \boldsymbol{e}_1^T(-\kappa_1\boldsymbol{e}_1 + \boldsymbol{e}_2) + \boldsymbol{e}_2^T(-\boldsymbol{e}_1 - \kappa_2\boldsymbol{e}_2) \\ &= -\kappa_1\boldsymbol{e}_1^T\boldsymbol{e}_1 + \boldsymbol{e}_1^T\boldsymbol{e}_2 - \boldsymbol{e}_2^T\boldsymbol{e}_1 - \kappa_2\boldsymbol{e}_2^T\boldsymbol{e}_2 \\ &= -\kappa_1\boldsymbol{e}_1^2 - \kappa_2\boldsymbol{e}_2^2\end{aligned} \tag{29}$$

Since $\kappa_1 > 0$, $\kappa_2 > 0$ and $\lambda > 0$, therefore $\dot{V} \leq 0$. For the Lyapunov function by Eq.(26), the unique origin are $\boldsymbol{e}_1 = \boldsymbol{0}$ and $\boldsymbol{e}_2 = \boldsymbol{0}$. The backstepping tracking control law (25) can stabilize the virtual tracking errors and converges to zero as a result of $V_1 \geq 0$ and $\dot{V}_1 \leq 0$.

Since $\lim_{t\to\infty} \boldsymbol{e}_1 = \mathbf{0}$ and $\lim_{t\to\infty} \boldsymbol{e}_2 = \mathbf{0}$, we can get $\lim_{t\to\infty} \tilde{\boldsymbol{x}}_1 = \mathbf{0}$ and $\lim_{t\to\infty} \tilde{\boldsymbol{x}}_2 = \boldsymbol{\xi}$ by Eq.(21). The backstepping tracking control law can guarantee the tracking error $\tilde{\boldsymbol{x}}_1$ to be stable and converge to zero. The rate of change of $\tilde{\boldsymbol{x}}_1$ should be steady when the $\tilde{\boldsymbol{x}}_1$ is converge to zero, $\dot{\tilde{\boldsymbol{x}}}_1 = \mathbf{0}$ when $t \to \infty$. Through Eq.(23), the $\boldsymbol{\xi} = \dot{\boldsymbol{x}}_{1d} - A\boldsymbol{x}_1 - \boldsymbol{x}_{2d}$ when the system converges to the steady state ($\boldsymbol{e}_1 = \mathbf{0}$).

Obviously, $\boldsymbol{x}_{1d}$ and $\boldsymbol{x}_{2d}$ should also satisfy the relationship as the dynamic equation Eq.(17), we can get $\dot{\boldsymbol{x}}_{1d} = A\boldsymbol{x}_{1d} + \boldsymbol{x}_{2d}$. Then Eq.(23) will be

$$\boldsymbol{\xi} = -\kappa_1 \boldsymbol{e}_1 + A\boldsymbol{x}_{1d} - A\boldsymbol{x}_1 = -(\kappa_1 I + A)\boldsymbol{e}_1 \tag{30}$$

Therefore, $\lim_{t\to\infty} \tilde{\boldsymbol{x}}_2 = \boldsymbol{\xi} = \mathbf{0}$. □

In this proof the fault and uncertainty are not taken into account. An improved control law is designed in the following section that is robust to both uncertainties and the defined faults. The virtual tracking error differential functions of the supercavitating vehicle (22) is used with the virtual control law given by Eq.(23).

Assumption 2. *Assuming the modeling parameter uncertainties $\Delta\bar{B}, \Delta\bar{C}$ and $\Delta\bar{\boldsymbol{F}}_p$ are bounded, $\left(\bar{C} + \Delta\bar{C}\right)\boldsymbol{\Gamma}_g\boldsymbol{u} - \bar{C}\boldsymbol{u}$ is bounded because of the output of the controller is limited in practice. It can be assumed that $\Delta\bar{B}\boldsymbol{x}_2$ is bounded. Considering the Assumption 1, the total uncertainties $\boldsymbol{E}_d$ is bounded and satisfied $|\boldsymbol{E}_d| \leq \boldsymbol{\rho}$, where $\boldsymbol{\rho} = [\rho_1, \rho_2]^T$, ρ_1 and ρ_2 are unknown bounded positive scalar.*

The following control law is proposed

$$\boldsymbol{u} = -\bar{C}^{-1}\left(\boldsymbol{e}_1 + \kappa_2\boldsymbol{e}_2 + \bar{B}\boldsymbol{x}_2 + \bar{\boldsymbol{F}}_g + \bar{\boldsymbol{F}}_p - \dot{\boldsymbol{x}}_{2d} - \dot{\boldsymbol{\xi}} + \Xi\left(\boldsymbol{e}_2\right)\hat{\boldsymbol{\rho}}\right) \tag{31}$$

$$\begin{aligned} \dot{\hat{\boldsymbol{\rho}}}\left(t\right) &= \lambda\left|\boldsymbol{e}_2\right| - \varepsilon\left(t\right)\hat{\boldsymbol{\rho}}\left(t\right) \\ \dot{\varepsilon}\left(t\right) &= -\gamma\varepsilon\left(t\right) \end{aligned} \tag{32}$$

where the function $\Xi\left(\boldsymbol{e}_2\right) = \mathrm{diag}\left[\mathrm{sign}\left(e_{21}\right), \mathrm{sign}\left(e_{22}\right)\right]$, $\mathrm{sign}\left(\cdot\right)$ is sign function. The control gain κ_2 is a positive scalar. The adaptive parameter $\hat{\boldsymbol{\rho}}$ is the estimated value of $\boldsymbol{\rho}$ which is the total uncertainties bound, the gains of the adaptive law λ and γ are positive scalars and the adaptive gain $\varepsilon\left(t\right)$ is positive because $\varepsilon\left(0\right) > 0$.

Theorem 2. *Under the virtual control law (23), the adaptive feedback control law (31) and adaptive update law (32), the supercavitating vehicle system Eq.(22) can guarantee its state to be uniformly ultimately bounded and to converge to a set* $\mathbf{\Omega}_1 = \left\{ \tilde{\boldsymbol{x}}_1 : \|\tilde{\boldsymbol{x}}_1\| \leq \|\hat{\boldsymbol{\rho}}\| \sqrt{\frac{\varepsilon(t)}{\Pi \cdot \lambda}} \right\}$ *and* $\mathbf{\Omega}_2 = \left\{ \tilde{\boldsymbol{x}}_2 : \|\tilde{\boldsymbol{x}}_2\| \leq \left(1 + \sqrt{2\kappa_1^2 + V^2}\right) \|\hat{\boldsymbol{\rho}}\| \sqrt{\frac{\varepsilon(t)}{\Pi \cdot \lambda}} \right\}$ *with* $\Pi = min\left\{2\kappa_1, 2\kappa_2, \varepsilon(t)\right\}$.

Proof: Defining the Lyapunov function as:

$$V_2 = \frac{1}{2}\boldsymbol{e}_1^T\boldsymbol{e}_1 + \frac{1}{2}\boldsymbol{e}_2^T\boldsymbol{e}_2 + \frac{1}{2\lambda}\tilde{\boldsymbol{\rho}}^T\tilde{\boldsymbol{\rho}} + \frac{\varepsilon}{\lambda\gamma}\boldsymbol{\rho}^T\boldsymbol{\rho} \tag{33}$$

where $\tilde{\boldsymbol{\rho}} = \boldsymbol{\rho} - \hat{\boldsymbol{\rho}}$.

The time derivative of the Lyapunov function is

$$\dot{V}_2 = {\boldsymbol{e}_1}^T\dot{\boldsymbol{e}}_1 + {\boldsymbol{e}_2}^T\dot{\boldsymbol{e}}_2 + \frac{\tilde{\boldsymbol{\rho}}^T\dot{\tilde{\boldsymbol{\rho}}}}{\lambda} + \frac{\dot{\varepsilon}}{\lambda\gamma}\boldsymbol{\rho}^T\boldsymbol{\rho} \tag{34}$$

Recalling Eq.(22) and Eq.(23), the time derivative of this Lyapunov function becomes

$$\dot{V}_2 = {\boldsymbol{e}_1}^T(-\boldsymbol{\kappa}_1\boldsymbol{e}_1 + \boldsymbol{e}_2) + {\boldsymbol{e}_2}^T(\bar{B}\boldsymbol{x}_2 + \bar{C}\boldsymbol{u} + \bar{\boldsymbol{F}}_g + \bar{\boldsymbol{F}}_p - \dot{\boldsymbol{x}}_{2d} - \dot{\boldsymbol{\xi}} + \boldsymbol{E}_d) + \frac{\tilde{\boldsymbol{\rho}}^T\dot{\tilde{\boldsymbol{\rho}}}}{\lambda} + \frac{\dot{\varepsilon}}{\lambda\gamma}\boldsymbol{\rho}^T\boldsymbol{\rho} \tag{35}$$

Substituting the control law Eq.(31) and Eq.(32) into Eq.(35) gives

$$\begin{aligned}
\dot{V}_2 &= \boldsymbol{e}_1^T\left(-\boldsymbol{\kappa}_1\boldsymbol{e}_1 + \boldsymbol{e}_2\right) + \boldsymbol{e}_2^T\left(-\boldsymbol{e}_1 - \boldsymbol{\kappa}_2\boldsymbol{e}_2 + \boldsymbol{E}_d - \Xi\left(\boldsymbol{e}_2\right)\hat{\boldsymbol{\rho}}\right) - \frac{\tilde{\boldsymbol{\rho}}^T\dot{\hat{\boldsymbol{\rho}}}}{\lambda} - \frac{\varepsilon}{\lambda}\boldsymbol{\rho}^T\boldsymbol{\rho} \\
&= -\boldsymbol{\kappa}_1\boldsymbol{e}_1^T\boldsymbol{e}_1 + \boldsymbol{e}_1^T\boldsymbol{e}_2 - \boldsymbol{e}_2^T\boldsymbol{e}_1 - \boldsymbol{\kappa}_2\boldsymbol{e}_2^T\boldsymbol{e}_2 + \boldsymbol{e}_2^T\boldsymbol{E}_d - \boldsymbol{e}_2^T\Xi\left(\boldsymbol{e}_2\right)\hat{\boldsymbol{\rho}} - \frac{\tilde{\boldsymbol{\rho}}^T}{\lambda}\left(\lambda\left|\boldsymbol{e}_2\right| - \varepsilon\left(t\right)\hat{\boldsymbol{\rho}}\right) - \frac{\varepsilon\left(t\right)}{\lambda}\boldsymbol{\rho}^T\boldsymbol{\rho} \\
&\leq -\boldsymbol{\kappa}_1\boldsymbol{e}_1^T\boldsymbol{e}_1 - \boldsymbol{\kappa}_2\boldsymbol{e}_2^T\boldsymbol{e}_2 + \sum_{i=1}^{2}|e_{2i}|\rho_i - \sum_{i=1}^{2}|e_{2i}|\hat{\rho}_i - \tilde{\boldsymbol{\rho}}^T\left|\boldsymbol{e}_2\right| + \frac{\varepsilon\left(t\right)}{\lambda}\tilde{\boldsymbol{\rho}}^T\hat{\boldsymbol{\rho}} - \frac{\varepsilon\left(t\right)}{\lambda}\boldsymbol{\rho}^T\boldsymbol{\rho} \\
&\leq -\boldsymbol{\kappa}_1\boldsymbol{e}_1^T\boldsymbol{e}_1 - \boldsymbol{\kappa}_2\boldsymbol{e}_2^T\boldsymbol{e}_2 + \tilde{\boldsymbol{\rho}}^T\left|\boldsymbol{e}_2\right| - \tilde{\boldsymbol{\rho}}^T\left|\boldsymbol{e}_2\right| - \frac{\varepsilon\left(t\right)}{2\lambda}\tilde{\boldsymbol{\rho}}^T\tilde{\boldsymbol{\rho}} - \frac{\varepsilon\left(t\right)}{2\lambda}\boldsymbol{\rho}^T\boldsymbol{\rho} + \frac{\varepsilon\left(t\right)}{2\lambda}\hat{\boldsymbol{\rho}}^T\hat{\boldsymbol{\rho}} \\
&= -\boldsymbol{\kappa}_1\boldsymbol{e}_1^T\boldsymbol{e}_1 - \boldsymbol{\kappa}_2\boldsymbol{e}_2^T\boldsymbol{e}_2 - \frac{\varepsilon\left(t\right)}{2\lambda}\tilde{\boldsymbol{\rho}}^T\tilde{\boldsymbol{\rho}} - \frac{\varepsilon\left(t\right)}{2\lambda}\boldsymbol{\rho}^T\boldsymbol{\rho} + \frac{\varepsilon\left(t\right)}{2\lambda}\hat{\boldsymbol{\rho}}^T\hat{\boldsymbol{\rho}} \\
&\leq -\Pi\cdot V_2 + \frac{\varepsilon\left(t\right)}{2\lambda}\|\hat{\boldsymbol{\rho}}\|^2
\end{aligned} \tag{36}$$

where $\Pi = min\left\{2\kappa_1, 2\kappa_2, \varepsilon(t), \frac{2}{\gamma}\right\}$ and $\|\cdot\|$ is Euclidean vector norm.

Solving Eq.(36), it can be obtained

$$V_2 \leq [V_2(0) - \frac{\varepsilon\left(t\right)}{2\lambda \cdot \Pi}\|\hat{\boldsymbol{\rho}}\|^2]\exp(-\Pi \cdot t) + \frac{\varepsilon\left(t\right)}{2\lambda \cdot \Pi}\|\hat{\boldsymbol{\rho}}\|^2 \tag{37}$$

The Lyapunov function V_2 is bounded. The following expression will be established when $t \to +\infty$

$$\lim_{t\to+\infty}(\frac{1}{2}\boldsymbol{e}_1^T\boldsymbol{e}_1 + \frac{1}{2}\boldsymbol{e}_2^T\boldsymbol{e}_2) \leq \lim_{t\to+\infty} V_2 \leq \frac{\varepsilon\left(t\right)}{2\lambda \cdot \Pi}\|\hat{\boldsymbol{\rho}}\|^2 \tag{38}$$

Recalling Eq.(21), $\|\tilde{\boldsymbol{x}}_1\| = \|\boldsymbol{e}_1\| \leq \sqrt{\frac{\varepsilon(t)}{\lambda\cdot\Pi}}\|\hat{\boldsymbol{\rho}}\|$ and $\|\tilde{\boldsymbol{x}}_2 - \boldsymbol{\xi}\| = \|\boldsymbol{e}_2\| \leq \sqrt{\frac{\varepsilon(t)}{\lambda\cdot\Pi}}\|\hat{\boldsymbol{\rho}}\|$. Simply, we can get $\|\tilde{\boldsymbol{x}}_2\| - \|\boldsymbol{\xi}\| \leq \|\tilde{\boldsymbol{x}}_2 - \boldsymbol{\xi}\| \leq \sqrt{\frac{\varepsilon(t)}{\lambda\cdot\Pi}}\|\hat{\boldsymbol{\rho}}\|$. Considering Eq.(30), this can be written as

$$\begin{aligned}\|\tilde{\boldsymbol{x}}_2\| &\leq \sqrt{\frac{\varepsilon\left(t\right)}{\lambda \cdot \Pi}}\|\hat{\boldsymbol{\rho}}\| + \|\boldsymbol{\xi}\| \\ &\leq \sqrt{\frac{\varepsilon\left(t\right)}{\lambda \cdot \Pi}}\|\hat{\boldsymbol{\rho}}\| + ||(\kappa_1 I + A)||_F||\boldsymbol{e}_1|| \\ &\leq \left(1 + \sqrt{2\kappa_1^2 + V^2}\right)\sqrt{\frac{\varepsilon\left(t\right)}{\lambda \cdot \Pi}}\|\hat{\boldsymbol{\rho}}\|\end{aligned} \tag{39}$$

where $||\cdot||_F$ is Frobenious matrix norms with $\|\cdot\|_F = \sqrt{\sum_{i=1}^{m}\sum_{j=1}^{n}|a_{ij}|^2}$. □

The nominal part of the discontinuous force calculated by (9) is eliminated by feedback. The uncertain part is included in the total uncertainty $\boldsymbol{E}_d$ as disturbance. The whole uncertain part is assumed to be unknown and bounded (assumption 2). It is treated by adaptive estimation law, as shown in (32).

4. Numerical Example

In this section, we will verify the effectiveness of the proposed control law (31) compared with the conventional backstepping control law in Eq.(40)

$$\boldsymbol{u} = -\left(\boldsymbol{e}_1 + \boldsymbol{\kappa}_2\boldsymbol{e}_2 + \bar{B}\boldsymbol{x}_2 + \bar{\boldsymbol{F}}_g + \bar{\boldsymbol{F}}_p - \dot{\boldsymbol{x}}_{2d} - \dot{\boldsymbol{\xi}}\right) \tag{40}$$

Table 1: Parameters of supercavitating vehicle model[3]

Parameters	Description	Value and units
g	Gravitational acceleration	$9.81m/s^2$
m	Density ratio	2
R_n	Cavitator radius	$0.0191m$
R	Vehicle radius	$0.0508m$
L	Vehicle length	$1.8m$
C_{x0}	Drag coefficient	0.82
n	Effectiveness of fins	0.5
V	Forward speed	$75m/s$
σ	Cavitation number	0.03

The multiplication fault model is given

$$g_i = \begin{cases} 1, & t < 5s \\ 0.8 + 0.1\cos(0.2\pi t), & t \geq 5s \end{cases} \tag{41}$$

the additive fault model is

$$\Gamma_{di} = \begin{cases} 0\,\text{deg}, & t < 5s \\ 0.01 + 0.01\sin(0.5\pi t)\,\text{deg}, & t \geq 5s \end{cases} \tag{42}$$

The initial conditions of the supercavitating vehicle are $z = 0m$, $w = 3m/s$, $\theta = -1\,\text{deg}$ and $q = 1\,\text{deg}/s$. The desired states of the supercavitating vehicle are $z = -1m$, $w = 0m/s$, $\theta = 0\,\text{deg}$ and $q = 0\,\text{deg}/s$. The parameters of the proposed control are $\boldsymbol{\kappa}_1 = [20, 20]^T$, $\boldsymbol{\kappa}_2 = [4, 4]^T$, $\lambda = 2$, $\gamma = 2$, $\varepsilon(0) = 20$, $\hat{\rho}_1(0) = 10$ and $\hat{\rho}_2(0) = 2$. The parameters of the supercavitating vehicle are given in Table 1, and the remaining parameters come from the CFD calculation results learned [38].

In order to test the tracking effectiveness of the proposed control law (31) more fairly, we will compare the pointing accuracy of the control law (31) and (40) for an ideal supercavitating vehicle model. From Fig.5 to Fig.8, the two control laws can accurately track the desired position and angle with no actuator faults and uncertainties in the model.

The robust tracking effectiveness of the proposed control law in presence of a multiplication fault (41),additive fault (42)and uncertainties is demonstrated in the following simulation. The comparison simulation results are as shown from Fig.9 to Fig.20.

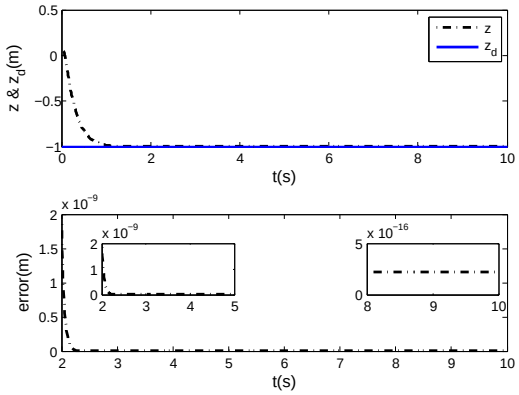

Figure 5: Position Tracking of proposed control

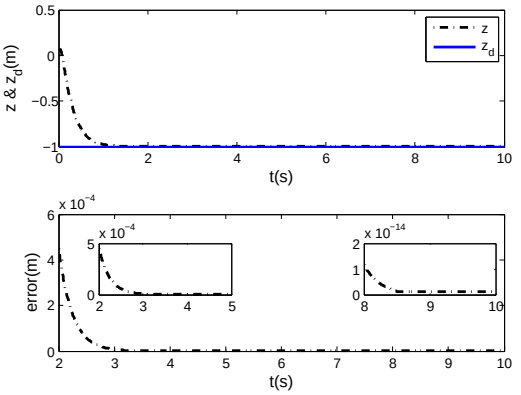

Figure 6: Position Tracking of compared control

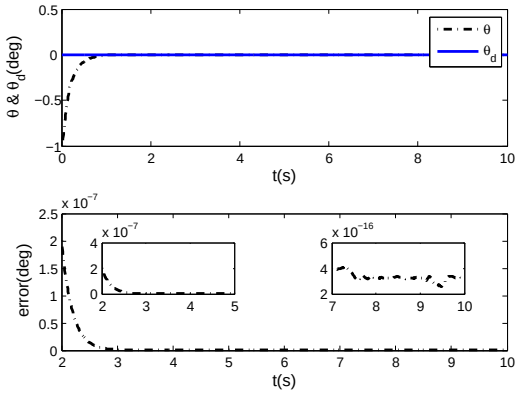

Figure 7: Angle Tracking of proposed control

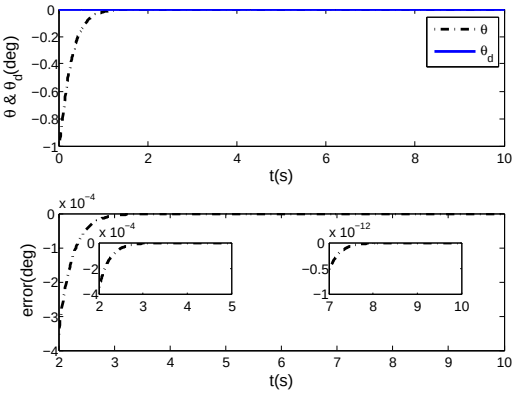

Figure 8: Angle Tracking of compared control

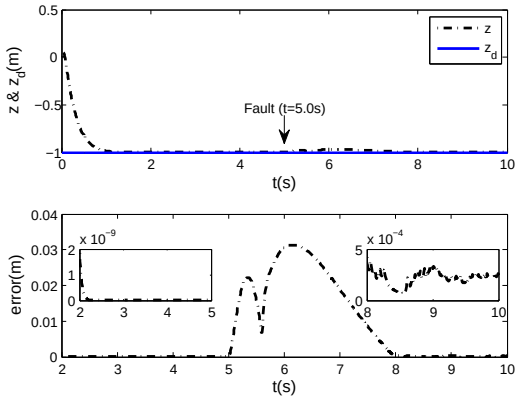

Figure 9: Position tracking of proposed control

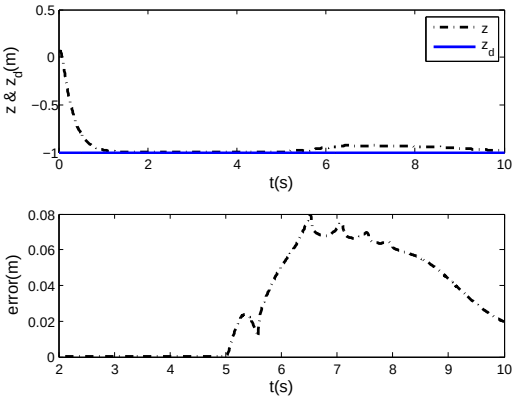

Figure 10: Position tracking of compared control

The back-stepping control shows poorer performance than the FTC. The position, angle, velocity and angular velocity do not track the desired value by using the conventional backstepping control (40). The corresponding results are shown in Fig.10, Fig.12, Fig.14 and Fig.16, respectively. However, the proposed control drives the tracking error to the zero error state which is only enabled by defining the adaptive component. The position tracks the desired value again by the dynamic adjusting from 5 second to 8 second. The tracking error is smaller than $5 \times 10^{-4} m$ shown in the Fig.9. The tracking errors of the angle, velocity and angular velocity converge to zero again after 1 second. Fig.11, Fig.13 and Fig.15 denote independently the corresponding results. The control torque of two methods are shown in Fig.17 and Fig.18. The adaptive gain is illustrated in Fig.19. The adaptive parameters are illustrated in Fig.20. The adaptive parameters $\hat{\rho}_1$ and $\hat{\rho}_2$ can converge to zero while the systems is normal. However, they can get a new value when the systems have faults to guarantee the accuracy. The capability of adjusting control parameters automatically using the system states is the key of the proposed control to deal with the actuator faults and uncertainties.

In order to verify the ability of the proposed control law to track continuous signals, the following simulation is undertaken. The depth and pitch angle tracking are considered, where the command signals are set as:

$$\begin{aligned} \dot{z}_d &= -\sin\theta(t) \\ \dot{\theta}_d &= \frac{\dot{z}_d}{V} \end{aligned} \tag{43}$$

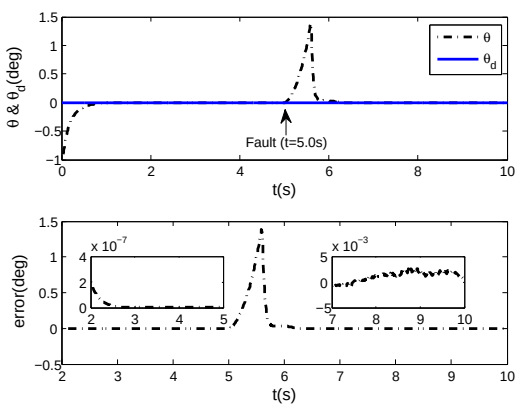

Figure 11: Angle tracking of proposed control

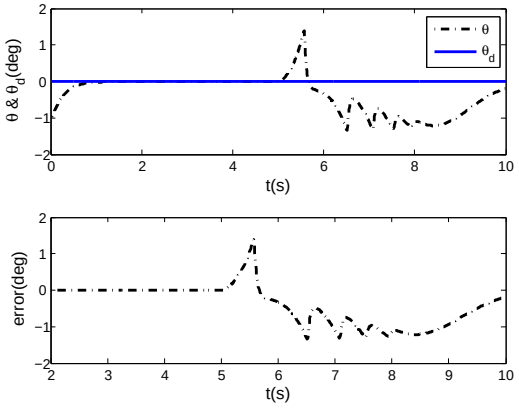

Figure 12: Angle tracking of compared control

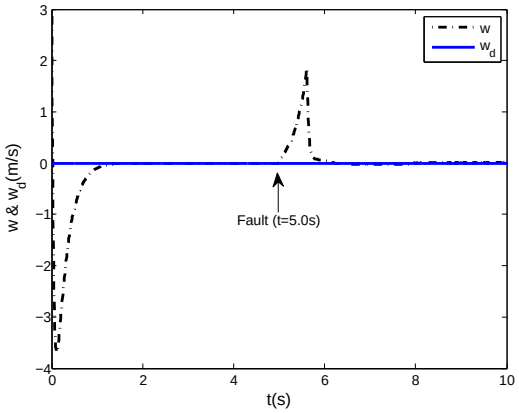

Figure 13: Velocity tracking of proposed control

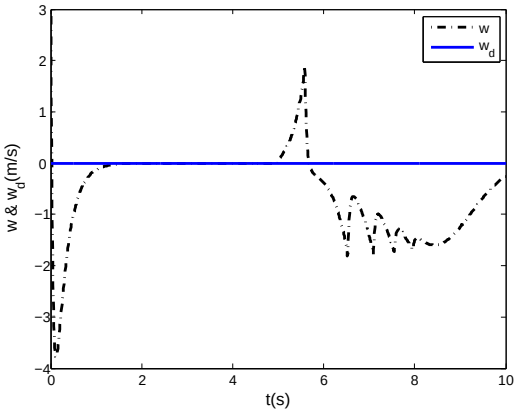

Figure 14: Velocity tracking of compared control

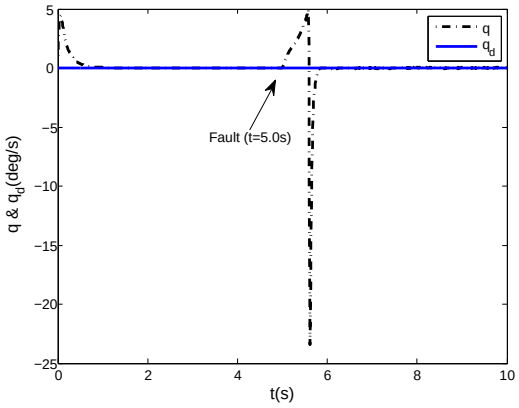

Figure 15: Angular velocity of proposed control

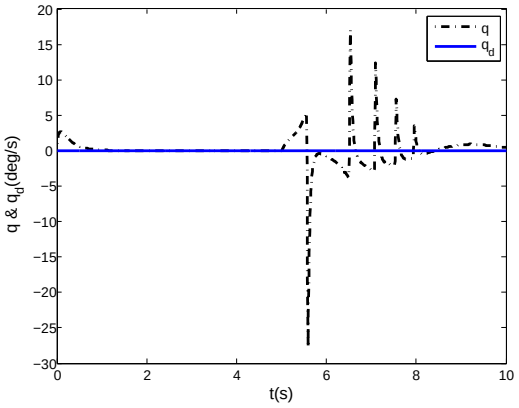

Figure 16: Angular velocity of compared control

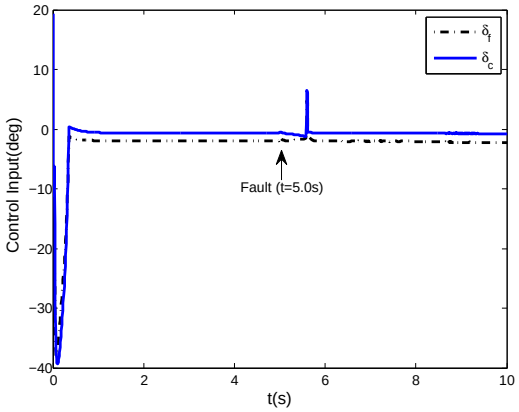

Figure 17: Control torque of proposed control

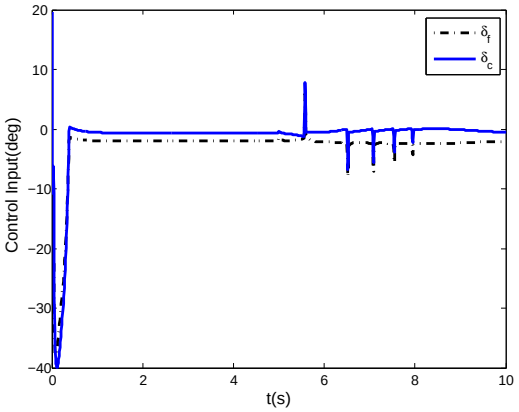

Figure 18: Control torque of compared control

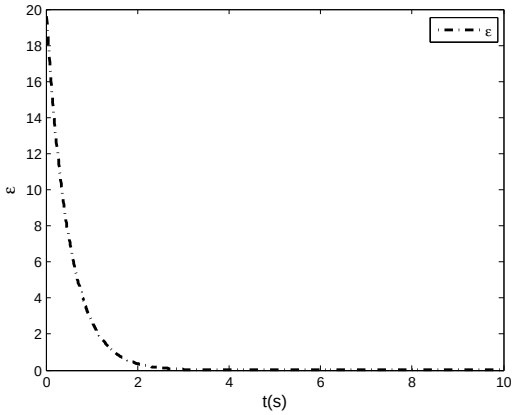

Figure 19: Adaptive gain of proposed control

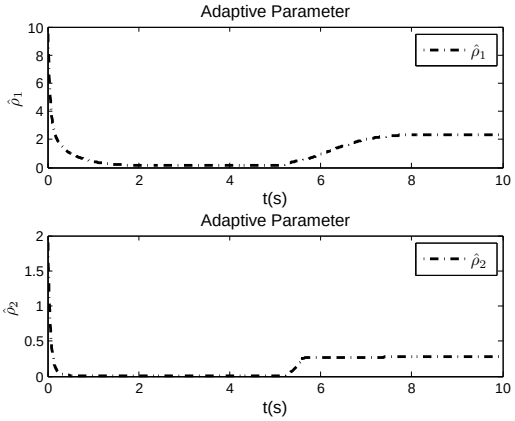

Figure 20: Adaptive parameters of proposed control

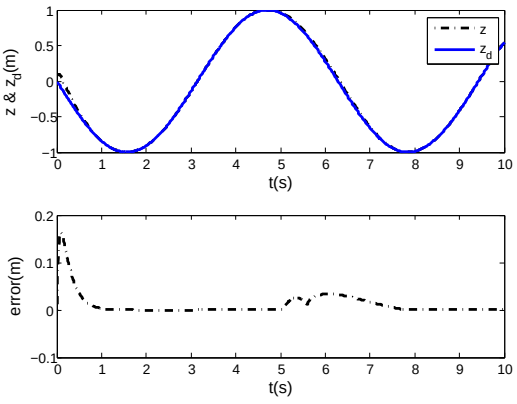

Figure 21: Position Tracking of proposed control(Continuous signals)

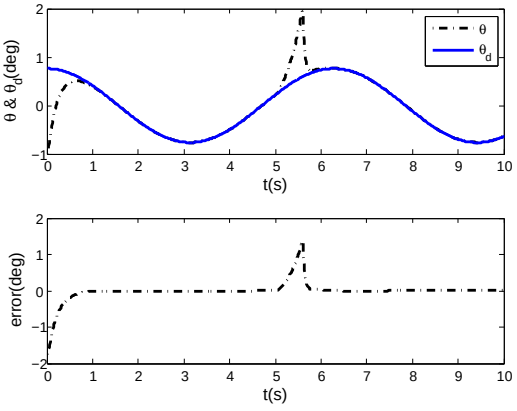

Figure 22: Angle tracking of proposed control(Continuous signals)

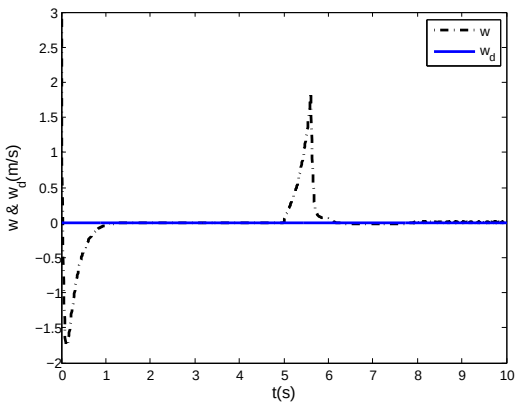

Figure 23: Velocity tracking of proposed control(Continuous signals)

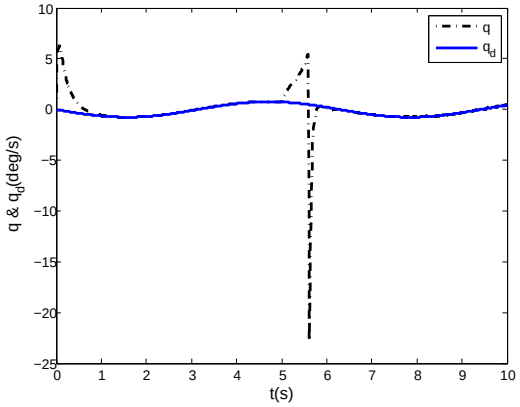

Figure 24: Angular velocity of proposed control(Continuous signals)

The initial conditions of the supercavitating vehicle and the parameters of the proposed control the same as above. The fault occurs in the 5th second. Tracking the time-varying signal results are shown in Fig.21-Fig.24. It can be seen from Fig.21 and Fig.22 that the proposed control law can achieve good tracking of continuous signals, which proves that it has the ability to track continuous signals. The tracking errors of the angle, velocity and angular velocity converge to zero again after 1 second in Fig.23, and Fig.24.

5. Conclusion

An adaptive backstepping tracking control law is developed for supercavitating vehicles which is robust to actuator failures, parameter, environmental uncertainties and actuator saturation limits. The closed-loop system stability is proved using a Lyapunov function and guarantees asymptotic tracking to a small, bounded region around the desired state in the presence of actuator faults and uncertainties. Numerical simulations demonstrate a significant improvement when compared to a classical backstepping control law in the presence of actuator faults and uncertainties.

Acknowledgments

This present research was supported by the National Nature Science Foundation of China(No. 61703125).

[1] Y. N. Savchenko."Supercavitation-Problems and Perspectives," *Fourth International Symposium on Cavitation*, California: California Institute of Technology, 2001. lecture.003.

[2] Ivan N. Kirschner and James S. Uhlman, "Overview of high-speed supercavitating vehicle control," *AIAA Guidance, Navigation, and Control Conference and Exhibit*, Keystone,Colorado, 2006, pp. 3100-3116. doi: 10.2514/6.2006-6442

[3] J. Dzielski and A. Kurdila, "A benchmark control problem for supercavitating vehicles and an initial investigation of solutions," *Journal of Vibration and Control*, Vol. 9, No. 7, 2003, pp. 791-804. doi: 10.1177/107754603031857

[4] G. L. Zhao, J.L. Fan and X.L. Lv, "Control of Supercavitating Vehicles in the Vertical Plane Using Sliding Mode," *2008 IEEE International Conference on Robotics and Biomimetics*, Bangkok, Thailand, 2009, pp. 1800-1805. doi: 10.1109/ROBIO.2009.4913275

[5] J.L. Fan, X.L. Lv, L. Su and G. L. Zhao, "Control of Supercavitating Vehicles Using Adaptive Integral Sliding Mode," *2009 IEEE International Conference on Mechatronics and Automation*, Changchun, China, 2009, pp. 4589-4593. doi: 10.1109/ICMA.2009.5244809

[6] M. Mirzaei, M. Eghtesad and M. M. Alishahi, "Planing force identification in high-speed underwater vehicles," *Journal of Vibration and Control*, Vol. 22, No. 20, 2016, pp. 4176-4191. doi: 10.1177/1077546315571660

[7] G.J. Lin, B. Balachandranand E. Abed, "Nonlinear dynamics and control of supercavitating bodies," *AIAA Guidance, Navigation, and Control Conference and Exhibit*, Keystone, Colorado, 2006, pp. 3151-3164. doi: 10.2514/6.2006-6445

[8] X.Y. Zhang, Y.H. Wei and Y.T. Han, et. al "Design and comparison of LQR and a novel robust backstepping controller for supercavitating vehicles," *Transactions of the Institute of Measurement and Control*, Vol. 39, No. 2, 2017, pp. 149-162. doi: 10.1177/0142331215607614

[9] S. Kim and N. Kim, "Neural network-based adaptive control for a supercavitating vehicle in transition phase," *Transactions of the Institute of Measurement and Control*, Vol. 20, No. 3, 2015, pp. 454-466. doi: 10.1007/s00773-014-0298-6

[10] X.F. Mao and Q. Wang, "Adaptive control design for a supercavitating vehicle model based on fin force parameter estimation," *Journal of Vibration and Control*, Vol. 21, No. 6, 2015, pp. 1220-1233. doi: 10.1177/1077546313496263

[11] I. Kirschner,D.C. Kring and A.W. Stokes, et.al "Control Strategies for Supercavitating Vehicles," *Journal of Vibration and Control*, Vol. 8, No. 2, 2002, pp. 219-242. doi: 10.1177/107754602023818

[12] G.J. Lin, B. Balachandranand E. Abed, "Dynamics and control of Supercavitating Vehicles," *Journal of dynamics system, measurement and control*, Vol. 130, No. 2, 2008, pp. 021003 1-11. doi: 10.1115/1.2837307

[13] B. Vanek and G.J. Balas, "Theoretical aspects of high-speed supercavitation vehicle control," *2006 American Control Conference*, Keystone, U.S.A., 2006, pp. 5263-5268. doi: 10.1109/ACC.2006.1657559

[14] B. Vanek and G.J. Balas, "Longitudinal Motion Control of a High-speed Supercavitation Vehicle," *Journal of Vibration and Control*, Vol. 13, No. 2, 2007, pp. 159-184. doi: 10.1177/1077546307070226

[15] B. Vanek, G.J. Balas and R.E.A. Arnd, "Linear, parameter-varying control of a supercavitating vehicle," *Control Engineering Practice*, Vol. 18, No. 9, 2010, pp. 1003-1012. doi: 10.1016/j.conengprac.2010.04.006

[16] X.F. Mao and Q. Wang, "Nonlinear Control Design for a Supercavitating Vehicle," *IEEE Transactions On Control Systems Technology*, Vol. 17, No. 4, 2009, pp. 816-832. doi: 10.1109/TCST.2009.2013338

[17] X.H. Zhao, Y.T. Han and T. Bai, et. al "H_∞ controller design using LMIs for high-speed underwater vehicles in presence of uncertainties and disturbances," *Ocean Engineering*, Vol. 104, 2015, pp. 359-369. doi: 10.1016/j.oceaneng.2015.05.026

[18] X.H. Zhao, Y. Sun and G.L. Zhao, et. al "μ-Synthesis robust controller design for the supercavitating vehicle based on the BT-T strategy," *Ocean Engineering*, Vol. 88, 2014, pp. 280-288. doi: 10.1016/j.oceaneng.2014.06.035

[19] X.Y. Zhang, K.M. Ma and Y.H Wei, et. al,"Finite-time robust H_∞ control for high-speed underwater vehicles subject to parametric uncertainties and disturbances," *Journal of Marine Science and Technology*, Vol. 22, No. 2 2017, pp. 201-218. doi: 10.1007/s00773-016-0404-z

[20] X.F. Mao and Q. Wang,"Delay-dependent control design for a time-delay supercavitating vehicle model," *Journal of Vibration and Control*, Vol. 17, No. 3, 2011, pp. 431-438. doi: 10.1177/1077546310366578

[21] Y. N. Savchenko,"Control of Supercavitation Flow and Stability of Supercavitating Motion of Bodies," *VKI Special Course on Supercavitation Flows*, Brussels: RTO-AVT ans VKI, 2001:313-341.

[22] Narula, A., Biggs, J. D."Fault-Tolerant Station-Keeping on Libration Point Orbits," *Journal of Guidance, Control, and Dynamics*, Vol. 41,

No. 4, 2018, pp. 879-887 doi: 10.2514/1.G003115

[23] Q.L. Hu, X. Tan and M.R. Akella,"Finite-Time Fault-Tolerant Spacecraft Attitude Control with Torque Saturation," *Journal of Guidance, Control, and Dynamics*, Vol. 40, No. 10, 2017, pp. 2524-2537. doi: 10.2514/1.G002191

[24] Y. Han, Biggs, J. D and N. G. Cui., "Adaptive Fault-Tolerant Control of Spacecraft Attitude Dynamics with Actuator Failures," *Journal of Guidance, Control, and Dynamics*, Vol. 38, No. 10, 2015, pp. 2033-2042. doi: 10.2514/1.G000921

[25] Q. Hu, B. Xiao, D. Wang and E. Poh, "Attitude Control of Spacecraft with Actuator Uncertainty," *Journal of Guidance, Control, and Dynamics*, Vol. 36, No. 6, 2013, pp. 1771-1776. doi: 10.2514/1.58624

[26] W. Cai, X. Liao and Y. Song, "Indirect Robust Adaptive Fault-Tolerant Control for Attitude Tracking of Spacecraft," *Journal of Guidance, Control, and Dynamics*, Vol. 31, No. 5, 2008, pp. 1456-1463 doi:10.2514/1.31158

[27] K. Lu and Y. Xia, "Finite-time fault-tolerant control for rigid spacecraft with actuator saturations," *IET Control Theory and Applications*, Vol. 7, No. 11, 2013, pp. 1529-1539. doi: 10.1049/iet-cta.2012.1031

[28] Q. Shen, D. Wang, S. Zhu and E. Poh, "Integral-Type Sliding Mode Fault-Tolerant Control for Attitude Stabilization of Spacecraft," *IEEE Transactions on Control Systems Technology*, Vol. 23, No. 3, 2015, pp. 1131-1138. doi: 10.1109/TCST.2014.2354260

[29] X. Huo, Q. Hu and B. Xiao, "Finite-Time Fault Tolerant Attitude Stabilization Control for Rigid Spacecraft," *ISA Transactions*, Vol. 53, No. 2, 2014, pp. 241-250. doi: 10.1016/j.isatra.2013.11.017

[30] Y Bai, JD Biggs, X Wang and N Cui, "Attitude Tracking with an Adaptive Sliding Mode Response to Reaction Wheel Failure," *European Journal of Control*, Vol. 41, No. 2, 2018, pp. 67-76. doi: 10.1016/j.ejcon.2018.02.008

[31] M.Z. Gao, G.P. Cai and Y. Nan, "Finite-Time Adaptive Fault-Tolerant Control for Airfoil Flutter of Reentry Vehicle," *Journal of Aerospace Engineering*, Vol. 31, No. 2, 2018, pp. 1-11. doi: 10.1061/(ASCE)AS.1943-5525.0000799

[32] Q. Dong, Q. Zong and B.L. Tian, et. al "Adaptive Disturbance Observer-based Finite-time Continuous Fault-tolerant Control for Reentry RLV," *International Journal of Robust And Nonlinear Control*, Vol. 27, No. 18, 2017, pp. 4275-4295. doi: 10.1002/rnc.3796

[33] Y. Zhang, S.J. Tang and J. Guo "Adaptive-Gain Fast Super-Twisting Sliding Mode Fault Tolerant Control for a Reusable Launch Vehicle in Reentry Phase," *ISA Transactions*, Vol. 71, 2017, pp. 380-390. doi: 10.1016/j.isatra.2017.08.012

[34] J.J. He and R.Y. Qi, et. al "Fault-tolerant Control with Mixed Aerodynamic Surfaces and RCS Jets for Hypersonic Reentry Vehicles," *Chinese Journal of Aeronautics*, Vol. 30, No. 2, 2017, pp. 780-795. doi: 10.1016/j.cja.2017.01.003

[35] W. Fan, H.H.T. Liu and R.H.S. Kwong, "Gain-Scheduling Control of Flexible Aircraft with Actuator Saturation and Stuck Faults," *Journal of Guidance, Control, and Dynamics*, Vol. 40, No. 3, 2017, pp. 510-520. doi: 10.2514/1.G002222

[36] R.C. Avram, X.D. Zhang and J. Muse, "Nonlinear Adaptive Fault-Tolerant Quadrotor Altitude and Attitude Tracking With Multiple Actuator Faults," *IEEE Transactions on Control Systems Technology*, Vol. 26, No. 2, 2018, pp. 701-707. doi: 10.1109/TCST.2017.2670522

[37] X. Yu, P. Li and Y.M. Zhang "The Design of Fixed-Time Observer and Finite-Time Fault-Tolerant Control for Hypersonic Gliding Vehicles," *IEEE Transactions on Industrial Electronics*, Vol. 65, No. 5, 2018, pp. 4135-4144. doi: 10.1109/TIE.2017.2772192

[38] Xulong Yuan and Tao Xing. "Hydrodynamic Characteristics of a Supercavitating Vehicle's Aft Body," *Ocean Engineering*, Vol. 114, 2016, pp. 37-46. doi: 10.1016/j.oceaneng.2016.01.012

[39] Zhao Xinhua. "Research on Dynamic Modeling and Control of Unerwater High-speed Vehicle," *Phd, Harbin Engineering University*, 2008, pp. 45-46. (In Chinese).

[40] Lv Rui. "Research on Dynamic Modeling and Robust Control of Supercavitating Vehicle During Attitude Maneuver," *Phd, Harbin Institute of Technology*, 2010, pp. 31-32. (In Chinese).